

# Classical versus quantum structure of the scattering probability matrix: Chaotic waveguides

G. A. Luna-Acosta,<sup>1</sup> J. A. Méndez-Bermúdez,<sup>1</sup> P. Šeba,<sup>2,3</sup> and K. N. Pichugin<sup>2,4</sup>

<sup>1</sup>*Instituto de Física, Universidad Autónoma de Puebla, Apartado Postal J-48, Puebla 72570, Mexico*

<sup>2</sup>*Department of Physics, University Hradec Kralove, Hradec Kralove, Czech Republic*

<sup>3</sup>*Institute of Physics, Czech Academy of Sciences, Cukrovarnicka 10, Prague, Czech Republic*

<sup>4</sup>*Kirensky Institute of Physics, 660036 Krasnoyarsk, Russia*

(Received 18 July 2001; published 25 March 2002)

The purely classical counterpart of the scattering probability matrix (SPM)  $|S_{n,m}|^2$  of the quantum scattering matrix  $S$  is defined for two-dimensional quantum waveguides for an arbitrary number of propagating modes  $M$ . We compare the quantum and classical structures of  $|S_{n,m}|^2$  for a waveguide with generic Hamiltonian chaos. It is shown that even for a moderate number of channels, knowledge of the classical structure of the SPM allows us to predict the global structure of the quantum one and, hence, understand important quantum transport properties of waveguides in terms of purely classical dynamics. It is also shown that the SPM, being an intensity measure, can give additional dynamical information to that obtained by the Poincaré maps.

DOI: 10.1103/PhysRevE.65.046605

PACS number(s): 05.45.-a, 89.75.Kd, 42.65.Wi

## I. INTRODUCTION

The  $S$  matrix is the most fundamental tool for analyzing quantum scattering phenomena in various fields of physics, for it provides us with the most complete scattering data [1]. Moreover, it is often of interest to extend the analysis to the semiclassical regime. The first semiclassical formulation of the  $S$  matrix appeared in the early 1970s in the works of Miller [2] and Marcus [3] in applications to atomic physics, and some years later extensions to their work were carried out by Heller [4]. Their common approach uses the Feynman propagator in the WKB approximation, thus taking into account classical dynamics together with quantum-mechanical interference, where the phases are given by the classical actions. In Ref. [5] some important further developments on the semiclassical treatment of scattering systems are listed. Quantum and semiclassical calculations of the  $S$  matrix have become essential for the understanding of transport phenomena in mesoscopic systems [6]. In particular, in the ballistic regime, the conductance is well described by the Landauer-Buttiker formula [7]  $G = (2e/\hbar^2) \sum_n \sum_m |t_{n,m}|^2$ , where  $t_{n,m}$  are the transmission elements of the  $S$  matrix. Semiclassical expressions for the transmission amplitudes for collinear leads were obtained by Jalabert, Baranger, and Stone [8] (see also Lin [9]).

One of the aims of studying ballistic motion in mesoscopic systems has been to relate the experimentally observed behavior of transport quantities, in the classical and quantum regimes, to their underlying classical dynamics [10]. This is particularly interesting when the associated classical dynamics can be chaotic; then the purpose is to identify signatures of chaos in the transport [11]. In a very recent example of this kind of work, Ketzmerick [12] showed that the fractal fluctuations of  $G$  as a function of magnetic field in a chaotic cavity are related to the Poincaré-Birkhoff hierarchical structure of the phase space of the corresponding classical motion. Previously, Baranger and co-workers [13] performed detailed quantum and semiclassical calculations of conductance in mesoscopic systems that display chaos in the classical regime. An important conclusion from their work is that

the behavior of the average conductance can already discern whether the underlying classical dynamics is regular or chaotic. Specially relevant for our purposes here is their finding that the dominant contributions to the average quantum conductance are classical. Thus it is natural to expect that useful information may be obtained by analyzing *purely* classical quantities, disregarding interference effects completely. Clearly, all the information contained in the phases of the quantum  $S$  matrix, necessary to calculate, e.g., the Wigner-Smith delay time, does not exist in the purely classical description. Nevertheless, as we shall show, important information can be extracted by studying the *scattering probability matrix* (SPM); its elements are defined by the square modulo of the  $S$ -matrix elements  $|S_{n,m}|^2$ , which give the transition probability for an incoming mode  $m$  to scatter into a mode  $n$ . The analysis of quantum and classical SP matrices is relevant also for the study of the wave-ray correspondence of electromagnetic fields propagating in cavities [14] since, under certain conditions, the wave equations are the same as for the quantum ballistic transport [15].

In this paper we shall construct the purely classical counterpart of the quantum SPM valid for any two-dimensional (2D) waveguide of arbitrary shape. Before doing so, in the following section we briefly review the definition of the  $S$  matrix in its application to cavities connected to leads. In Sec. III we construct the classical SPM and compare its quantum and classical structures for a model of a mesoscopic ballistic 2D waveguide that displays generic chaos in the classical limit. We shall show that the good global correspondence between classical and quantum SPM enables us to understand the classical dynamical origin of features of the quantum SPM and to clearly identify the differences produced by the wave nature of the quantum state. In Sec. IV, we make some concluding remarks.

## II. S MATRIX FOR WAVEGUIDES

The  $S$  matrix relates incoming waves to outgoing waves,

$$V^{\text{out}} = \hat{S} V^{\text{in}}, \quad (1)$$

where  $V^{\text{in}}$  and  $V^{\text{out}}$  stand for vectors specifying, respectively, waves coming into and going out of the interaction region. For a system composed of a 2D waveguide of arbitrary shape connected to two leads, say left ( $L$ ) and right ( $R$ ) leads, the solutions in the leads are

$$\Psi^{L,R}(x,y) = \sum_{m=1} [a_m^{L,R} \exp(ik_m^{L,R}x) + b_m^{L,R} \exp(-ik_m^{L,R}x)] \phi_m^{L,R}(y), \quad (2)$$

where

$$\phi_m^{L,R}(y) = \left(\frac{2}{d_{L,R}}\right)^{1/2} \sin\left(\frac{m\pi y}{d_{L,R}}\right) \quad (3)$$

is the component of the wave function along the  $y$  axis, perpendicular to the direction of propagation ( $x$  axis);  $d_L$  stands for the constant width of the left lead, which may be different from the width  $d_R$  of the right lead. For simplicity we shall use  $d_L = d_R$  for the rest of the paper. The sum is over all the propagating modes supported by the leads at a given Fermi energy  $E$ .

With this notation the  $S$  matrix and the incoming and outgoing waves can be written in the form

$$\hat{\mathbf{S}} = \begin{pmatrix} t & r' \\ r & t' \end{pmatrix}, \quad V^{\text{in}} = \begin{pmatrix} a^L \\ b^R \end{pmatrix}, \quad V^{\text{out}} = \begin{pmatrix} a^R \\ b^L \end{pmatrix}.$$

The symbols  $t$ ,  $t'$ ,  $r$ , and  $r'$  in the  $S$  matrix are  $M \times M$  matrices, where  $M$  is the highest mode (given by the largest  $m$  beyond which the longitudinal wave vector

$$k_m^{L,R} = \sqrt{2m_e E / \hbar^2 - m^2 \pi^2 / d_{L,R}^2}$$

becomes complex). The symbols  $a^{L,R}$  and  $b^{L,R}$  stand for the vectors  $a_m^{L,R}$  and  $b_m^{L,R}$ ,  $m = 1, 2, \dots, M$ . The *squared* modulo element  $|t_{n,m}|^2$  ( $|t'_{n,m}|^2$ ) gives the probability amplitude for a left (right) incoming mode  $m$  to be transmitted to the right (left) lead into the mode  $n$ . Similarly,  $|r_{n,m}|^2$  ( $|r'_{n,m}|^2$ ) is the probability for a left (right) incoming mode  $m$  to be reflected to the left (right) lead into mode  $n$ .

The quantum SPM is simply defined as  $|S_{n,m}|^2$ ; it gives the transition probability for the incoming mode  $m$  to scatter into an outgoing mode  $n$ .

### III. CLASSICAL SCATTERING PROBABILITY MATRIX

Since the energy of the system is given by its expression in the leads,

$$E = \frac{\hbar^2}{2m_e} \left( k_m^2 + \frac{m^2 \pi^2}{d^2} \right), \quad (4)$$

classically we can associate an angle  $\theta_m$  between the longitudinal component of the momentum  $k_m$  and the total momentum  $\sqrt{2m_e E / \hbar}$ . That is,

$$\theta_m = \sin^{-1} \left[ \frac{m\pi\hbar}{d\sqrt{2m_e E}} \right]. \quad (5)$$

For a finite number  $M$  of modes there corresponds a range of angles  $\Delta\theta_m \equiv \theta_m - \theta_{m-1}$  for each mode  $m$ . The classical limit is of course  $M = \infty$ .

Consider a classical particle entering, say, from the left side and making an angle  $\theta_i$ , within a range corresponding to a given mode  $m$ . The particle (ray) will generally collide with the walls of the waveguide a few times before exiting to the left or to the right, making a certain angle  $\theta_f$ , to which we can associate a mode  $n$  if  $\theta_f \in \Delta\theta_n$ . Initial conditions are specified not just by the angle but also by the initial position  $(x,y)$  along the left lead. In order to account for all possible types of trajectories, we take a large number of initial positions for each incoming angle  $\theta_i$ . By recording the number of particles scattered into the various ranges of  $\theta$  associated with different outgoing modes  $n$ , we obtain a distribution of outgoing modes for each incoming mode  $m$ . This distribution gives the *classical counterpart* of the matrix elements  $|t_{n,m}|^2$  and  $|r_{n,m}|^2$  of the quantum SPM. Similarly, to obtain the classical counterparts of  $|t'_{n,m}|^2$  and  $|r'_{n,m}|^2$  we repeat the above process but for particles entering from the right lead. This defines the procedure to construct the *classical counterpart* of the SPM.

Clearly, the semiclassical regime is defined by  $\lambda/a \ll 1$ , where  $\lambda$  is the de Broglie wavelength. To get an expression of this condition in terms of the number of open modes  $M$  for a given energy, we use the formula for the energy in the leads,

$$E = \frac{\hbar^2}{2m_e} \frac{(2\pi)^2}{\lambda^2} \approx \frac{\hbar^2}{2m_e} \frac{(M\pi)^2}{d^2}.$$

Here we neglected the value of the longitudinal wave vector  $k_m^{L,R}$ . This gives  $\lambda = 2d/M$  and the condition  $\lambda/a \ll 1$  gives  $M \gg 2d/a$ . Below, when we compare quantum and classical calculations, we shall see how large this inequality should be in order to get a decent quantum-classical correspondence (QCC).

#### A. The waveguide model

We now specify a waveguide model on which to explore the quantum and classical structures of the SPM. We choose the geometry of the waveguide to be that of a ‘‘rippled’’ billiard, shown in Fig. 1, which is connected to two collinear leads of the same width. As a prototype of a quantum or electromagnetic waveguide, it has been used to study certain transport manifestations of chaos in the classical [16,17] as well as quantum [18] regimes. On the other hand, the infinitely long (i.e., periodic) version of the rippled billiard, introduced first in connection with beam acceleration problems [16,19], has been useful also for the understanding of typical features of crystals (e.g., energy band structure, LDOS, etc.) and their quantum-classical correspondence [20–22].

Although, as a scattering system, the *finite* version of the rippled channel is the relevant one, it is convenient first to

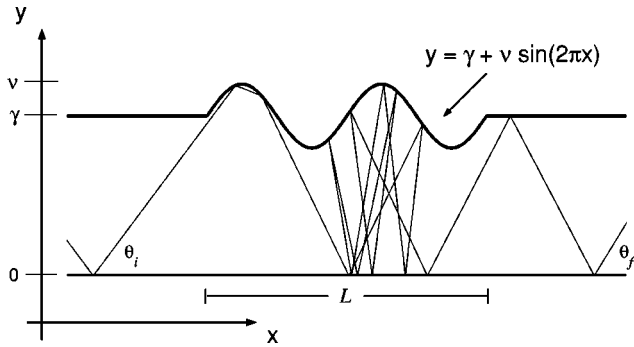


FIG. 1. Geometry of the waveguide.

review briefly the motion in the infinitely long rippled billiard,  $L \rightarrow \infty$ . As usual, to get the dynamical panorama, we look at a Poincaré map of the system. As the Poincaré surface of section, we choose, for reasons of symmetry, the bottom boundary  $y=0$ ; the Poincaré map is given by the pair of Birkhoff variables  $(x_j, \theta_j)$ , labeling the longitudinal components of the position and angle of the particle right after its  $j$ th collision with the bottom wall. Since the channel is periodic, the Poincaré map is on the cylinder [i.e.,  $x(\text{mod } 1)$ ]. Depending on the geometrical parameters (average width  $\gamma$  and amplitude  $\nu$  of the ripple) the dynamics is either regular, mixed, or fully chaotic. Figures 2(a) and 2(b) show, respectively, typical Poincaré sections for a wide ( $\gamma = 0.5, \nu = 0.12$ ) and a narrow ( $\gamma = 0.25, \nu = 0.025$ ) channel. In general, for small amplitudes of the ripple ( $\nu \ll 1$ ) wide channels ( $\gamma \gtrsim \frac{1}{2}$ ) give rise to global chaos, whereas narrow channels yield mixed dynamics, as exemplified by Figs. 2(a) and 2(b). For future reference in this paper we shall denote the system displaying globally chaotic dynamics ( $\gamma = 0.5, \nu = 0.12$ ) as the *G system* and the mixed one ( $\gamma = 0.25, \nu = 0.025$ ) as the *M system*.

Since the Poincaré plots of the *periodic* rippled billiard show topological chaos (i.e., a heteroclinic tangle), it is not surprising that a *finite* rippled billiard connected to the leads shows chaotic scattering, as evidenced by the fractal nature of its scattering functions [17]. In fact, as is well known [23], topological chaos is responsible for the fractality of the scattering functions.

#### IV. RESULTS

In the following we shall compare the quantum and classical SP matrices for both systems, *G* and *M*, and for various lengths of a rippled waveguide. In all cases we will consider energies that allow for 33 propagating modes.

##### A. The *G system*

Figures 3(a) and 3(b) show, respectively, the quantum and classical SPM for the rippled waveguide whose length equals one period of the ripple ( $L=1$ ). The resemblance between the classical and quantum SP matrices is remarkable. Let us consider first the reflection part of the SP matrices, say the left bottom block  $|r_{n,m}|^2$ . Notice, in the classical SPM, the high intensity in the neighborhood of the  $(n,m)=(11,11)$

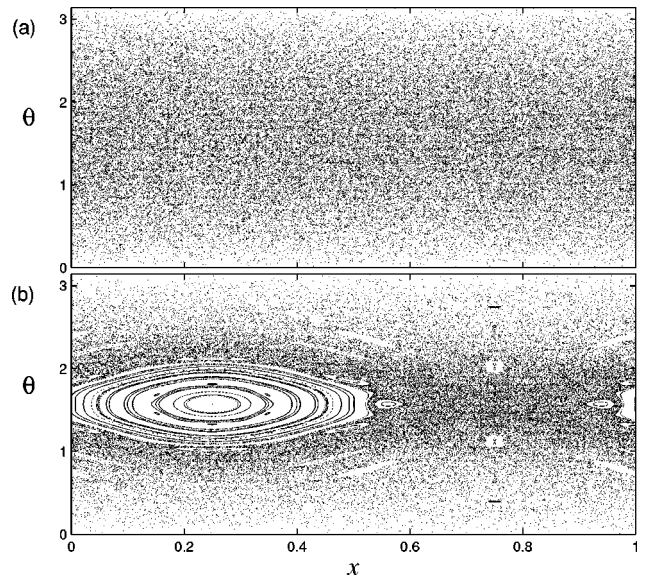


FIG. 2. Poincaré surface of section at  $\gamma=0$  for (a)  $(\gamma, \nu) = (0.5, 0.12)$  and (b)  $(\gamma, \nu) = (0.25, 0.025)$ .

element and along a hyperbolalike curve centered on it. The quantum SPM also shows the same pattern. The same is true for the conelike shape starting at the  $(n,m)=(11,11)$  element. More impressive is the similitude of triangular shapes near the top right corner. This global correspondence enables us to predict, based solely on the classical pictures, important quantum transport features. For example, the classical SPM predicts that there will be negligible reflection for modes  $m \leq 4$ . This is confirmed in Fig. 4, which shows in detail how the incoming modes 2 and 3 do not reflect, whereas the incoming mode number 5 does reflect partially into the outgoing mode number 24, just as predicted classically [note the high-intensity element  $(n,m)=(24,5)$ ]. These figures also show that the modes 2, 3, and 5 transmit predominantly onto the same modes as the incoming ones; this would be just like the classical probabilities except that the quantum one shows, in addition, small transmission to some modes off the diagonal. Detailed analysis of the data shows that the classical SPM also gives transmission off the diagonal but it is not evident because their intensity is weak and almost uniform over all modes. This difference is due to quantum interference, which is also responsible for the larger width of the diagonal elements of the transmission parts. As another example, the classical SPM predicts that mode 11, incoming from the left, will reflect and transmit predominantly onto the same channel number, which is confirmed by Fig. 4(b).

It is instructive to identify the type of trajectories that form the most salient features of the classical SPM since these are also evident in the quantum SPM. As an illustration, the triangular shape (see Fig. 5) that appears near the top right corner of the  $|r_{n,m}|^2$  block results from incoming trajectories colliding only *once* with the rippled boundary in the neighborhood of  $x = \frac{1}{2}$ , the hyperbolalike curve and also the conelike shape are formed by trajectories colliding *twice* with the rippled boundary.

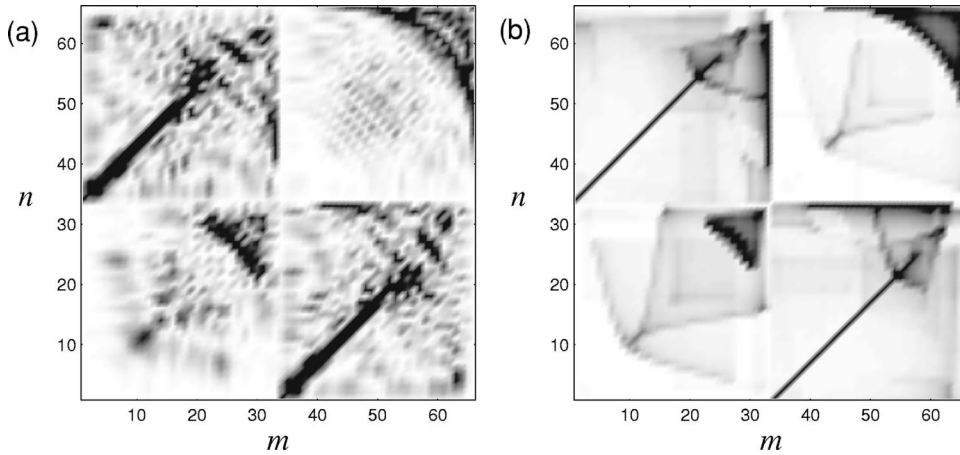


FIG. 3. (a) Quantum and (b) classical SPM,  $|S_{n,m}|^2$ , for the one-period waveguide with  $(\gamma, \nu) = (0.5, 0.12)$ .

An important aspect of the quantum-classical correspondence, which was not expected, is the particlelike behavior that results from the interaction with the rippled waveguide of certain plane waves. As an example, Fig. 6 illustrates this behavior for the incoming waves with mode numbers 24 and 29. Note that a high-intensity pattern is formed on the left side of the rippled waveguide, resembling a ray trace. The angle this pattern makes with the horizontal, labeled  $\alpha$  in the figure, corresponds precisely with the angle of reflection predicted by the classical SPM. In general, we see that when there is a *high-intensity* element in the classical SPM one can expect the wave function to form a ray pattern along the classical trajectory just outside the cavity. This may be regarded as a “short-lived scar.”

In contrast, when the classical SPM shows *homogeneous areas of low intensity* probabilities, the quantum SPM is ex-

pected to show a mottled pattern of medium-intensity probabilities. A homogeneous area of low-intensity classical probabilities results when incoming particles within a range  $\Delta\theta_m$  scatter uniformly throughout a much wider range of angles. This effect, the defocusing caused by the rippled boundary, is responsible for the strong sensitive dependence to initial conditions, the main ingredient of chaos. Clearly, the larger the number of periods forming the rippled waveguide, the stronger this effect should be. Figures 7(a) and 7(b), showing the quantum and classical SP matrices for the same geometry as just above ( $\gamma=0.5, \nu=0.12$ ), but six times longer ( $L=6$ ), confirm this expectation for the *transmission* parts. Comparison of the classical SP matrices [Figs. 3(b) and 7(b)] shows that, with the exception of a high-intensity spot near the transmission element  $(n,m)=(28,28)$  and a short diagonal contribution  $(n,m)<(5,5)$ , all the distin-

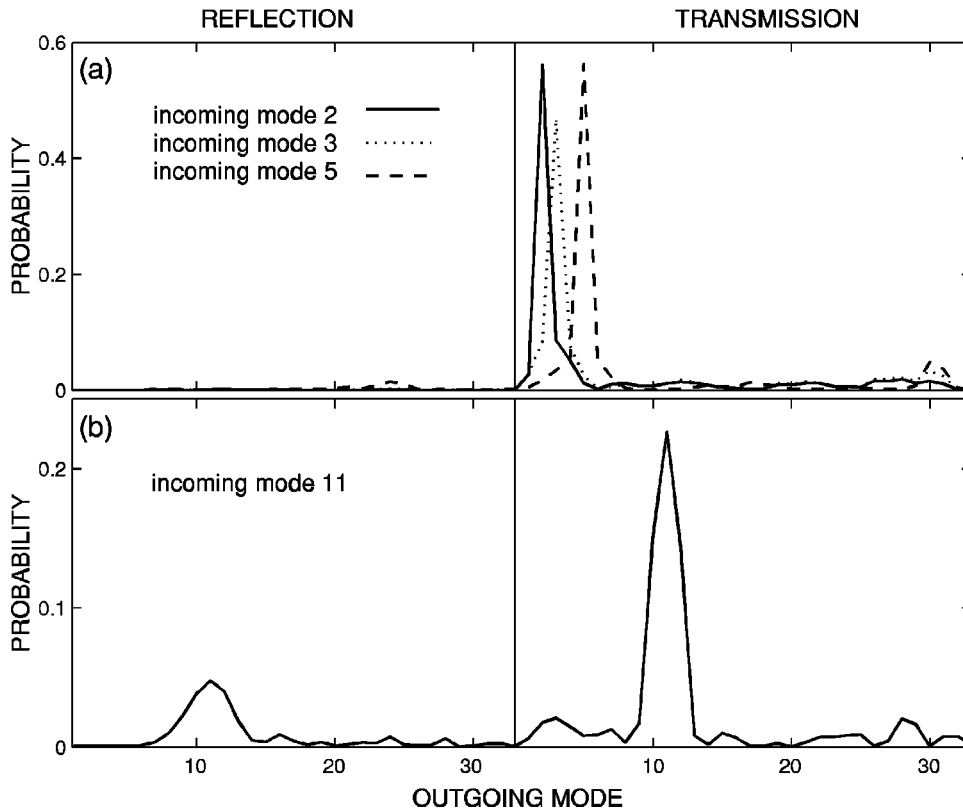


FIG. 4. Reflection and transmission probabilities from the classical SPM for (a) the incoming modes 2, 3, 5 and (b) 11. The one-period waveguide with  $(\gamma, \nu) = (0.5, 0.12)$  is considered.

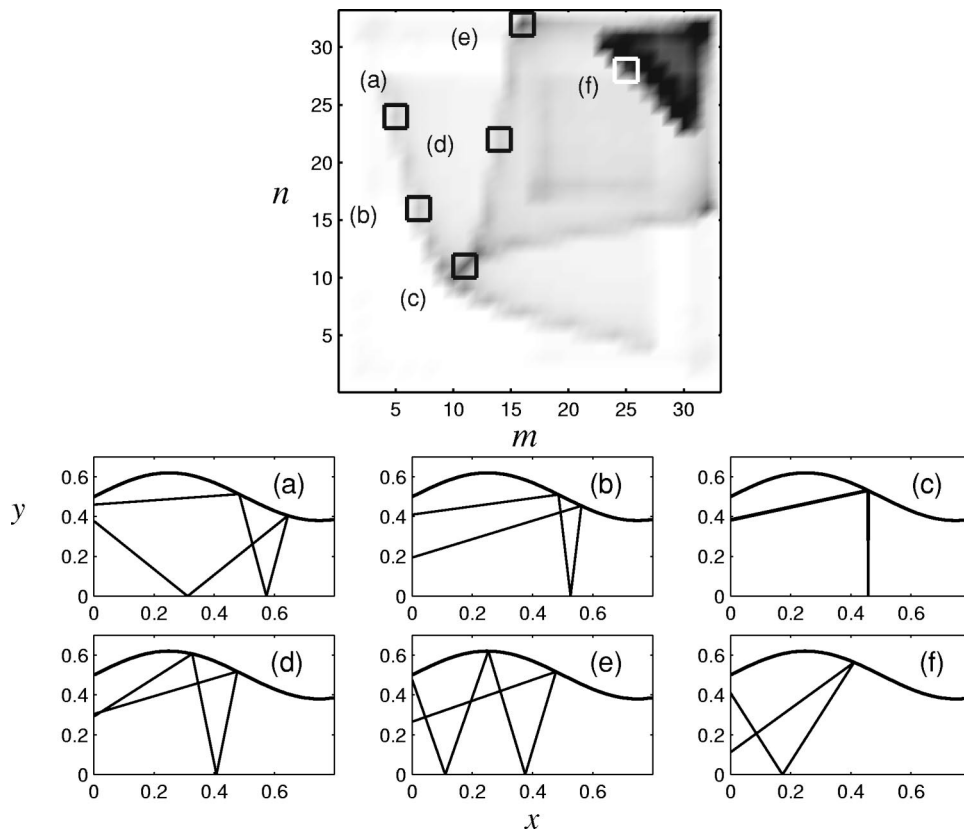


FIG. 5. Typical types of trajectories that contribute to the zones marked in the reflection part  $|r_{n,m}|^2$  of the classical SPM of Fig. 3.

guishing features of the transmission parts obtained for a one-period-long waveguide [Fig. 3(b)] are washed out in the case of the six-period-long waveguide. The remaining high-intensity diagonal elements for low modes are due to direct transmission, i.e., to trajectories that transmit without colliding with the upper wall. To get an estimate for the number of incoming modes that transmit predominantly onto the same mode, we assume flat boundaries (since the amplitude of the ripple is small compared to the width  $\gamma$ ) and consider a

bundle of particles injected at  $(x, y) = (0.0, 0.5)$ . The particles can transmit directly (no collisions with upper or lower boundary) if their initial angle  $\theta_i$  is in the interval  $(-\theta_c, \theta_c)$ , where  $\theta_c \equiv \tan^{-1}(2L/d)$ , and  $L$  is the length of the channel. For the one-period-long and six-period-long waveguide, these angles are, respectively, 0.46 and 0.083 rad. The ratio  $\sin(0.083)/\sin(0.46)$  is 0.18, which agrees with the ratio between the lengths of the high-intensity diagonals in the transmission of Figs. 3(b) and 7(b).

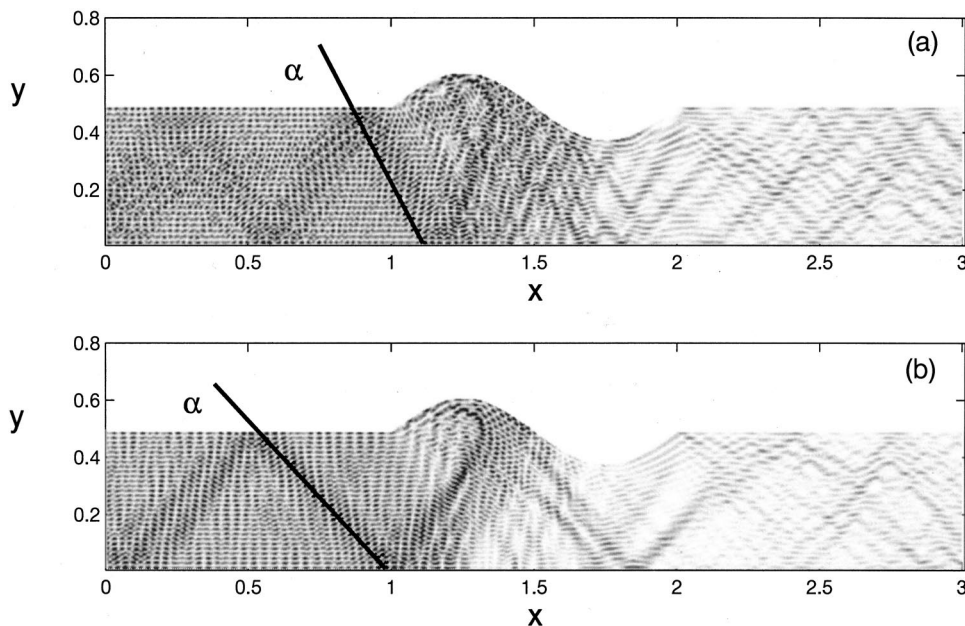


FIG. 6. Wave function of the incoming mode (from the left) number (a) 24 and (b) 29. (a)  $\alpha \sim 60^\circ$  and (b)  $\alpha \sim 47^\circ$  are the reflection angles predicted by the classical SPM of Fig. 3.

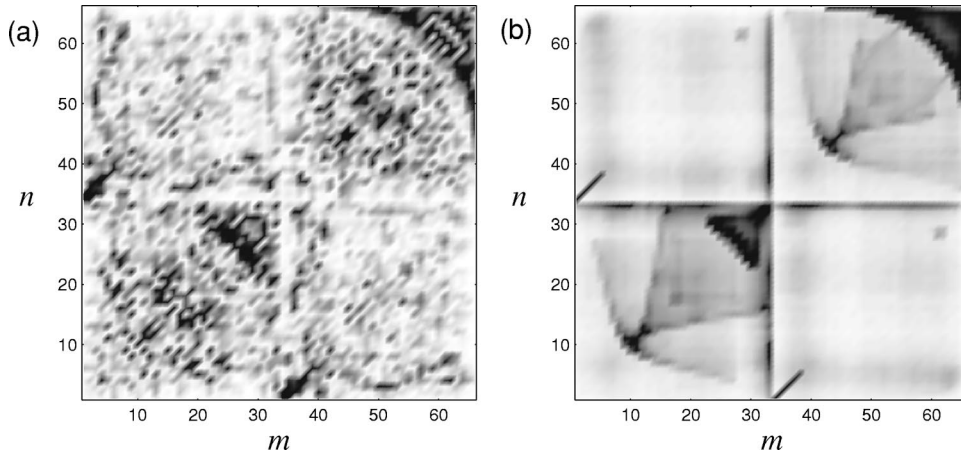


FIG. 7. (a) Quantum and (b) classical SPM,  $|S_{n,m}|^2$ , for the six-period waveguide with  $(\gamma, \nu) = (0.5, 0.12)$ .

We remark that the homogeneous spread of intensities in the transmission part of the classical SPM for  $(n, m) > (5, 5)$  is consistent with the “equal *a priori* distribution” of the  $S$  matrix required for the validity of the random  $S$ -matrix theory approach to chaotic cavities [24]. But note that in the reflection parts of the classical SPM the inhomogeneity is especially strong. In fact, while the definite transmission structures of the one-period waveguide have been somewhat washed out in the six-period waveguide, classically, the reflection blocks remain practically the same as for the one-period-long waveguide. This is because the reflection structures are mainly formed by particles reflecting within the first period of the ripple, see Fig. 5. On the other hand, backscattering after the first period of the rippled waveguide shows up classically as an almost homogeneous spread of intensity throughout the reflection blocks (including the area below the hyperbolalike curve for which there was no reflection for the one-period waveguide). Thus, while classically the definite pattern produced by the first period of the wave-

guide persists, quantum interference of the backscattering from the whole waveguide starts to destroy the pattern observed in the classical SPM.

Another interesting feature comes from the analysis of the relatively bright spot observed in the transmission part of the classical SPM near the site  $(n, m) = (28, 28)$ . An enlargement of this spot is shown in Fig. 8(a) and a typical trajectory belonging to this pattern is shown in Fig. 8(c). The distinctive feature of these types of trajectories is that they collide twice with the rippled boundary for each bounce with the flat boundary. These are periodic or quasiperiodic orbits advancing always to the right and form the stability island surrounding the stable period-one fixed point shown in Fig. 8(b). It is important to remark that this miniscule Poincaré-Birkhoff structure (note the scale of the axis) is not visible in the whole Poincaré map of Fig. 2(a), even though its effect is clearly manifested in the classical SPM. Hence, we see that the SPM construction can give complementary information to that obtained by the Poincaré maps because it is an inten-

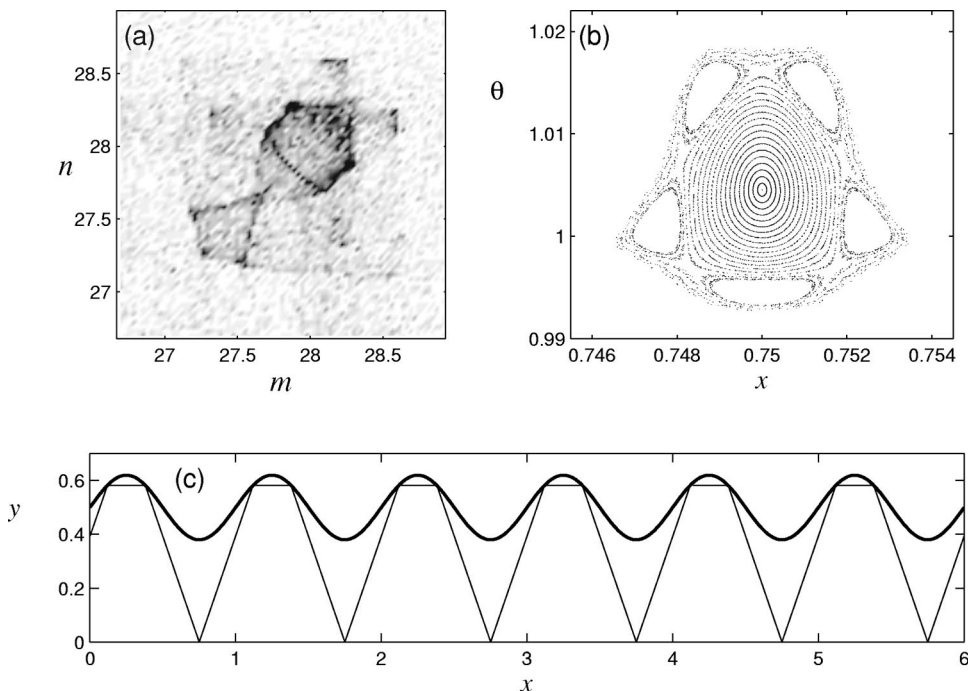


FIG. 8. (a) Enlargement of the transmission part of the classical SPM around the site  $(n, m) = (28, 28)$ . (b) Phase space generated by the trajectories that produce the structure of (a). (c) Typical orbit belonging to the pattern in (a).

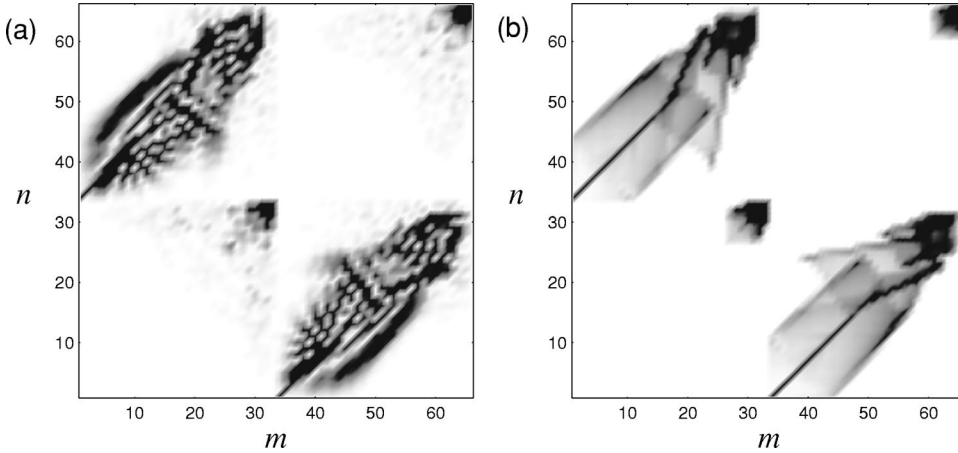


FIG. 9. (a) Quantum and (b) classical SPM,  $|S_{n,m}|^2$ , for the one-period waveguide with  $(\gamma, \nu) = (0.25, 0.025)$ .

sity measure. On the other hand, such a spot is not present in the quantum SPM because the size of the Poincaré-Birkhoff structure is too small to be resolved quantum mechanically (there are other spots visible but they do not correspond to the classical one; they originate from constructive interference).

### B. The $M$ system

Now we examine briefly the classical and quantum SP matrices for the  $M$  system. Figures 9(a) and 9(b) show these matrices for a one-period-long waveguide. Again, a quick comparison of these shows that the global features of the quantum SPM can be predicted by the classical SPM. We see that regions of high-intensity areas in the quantum SPM correspond roughly to the high-intensity areas of the classical SPM, albeit fluctuations within them. However, there are some important differences that we shall discuss now. Note that both classical and quantum SP matrices show that reflection occurs only for high modes but the classical reflection occurs only for modes higher or equal to  $m=31$  while quantum reflection (although weak) exists even for modes as low as  $m=10$ . The mechanism responsible for the reflection of classical particles can be understood by examining the Poincaré map of the infinitely long channel, Fig. 2(b), which shows a large resonance island centered at  $x=\frac{1}{4}$ . This resonance is produced by trajectories executing librational motion, bouncing between the two walls in the neighborhood of the widest part of the channel,  $x=\frac{1}{4}$ . It is clear then that particles entering the rippled waveguide from the left at  $x=0$  can reflect (after one or several bounces) within the *first period* of the channel if their trajectories fall within the resonance island. Trajectories falling on the chaotic sea outside the resonance island (hence low transversal mode numbers) can also reflect via the chaotic separatrix but not within the first period of the ripple. The longitudinal momentum of these librational orbits is relatively small [see Fig. 2(b)], hence their transverse momentum is large. Detailed analysis using Eq. (5) and data from Fig. 2(b) shows that indeed the lowest mode that can reflect is  $m=31$ , in agreement with Fig. 9(b). In contrast there is a strong quantum reflection for modes as low as  $m=25$ . Heisenberg's uncertainty principle is responsible for this difference. Namely, the quantum state cannot resolve the fine classical boundaries defining the reso-

nance island and consequently even smaller values of  $m$  can “tunnel” into the resonance island to cause partial reflection.

As regards the usefulness of our classical approach, we recall that good QCC is expected for  $M \gg 2d/a$ . For the  $G$  system, where  $2d/a \approx 8$ , our calculations showed that already for  $M=33$  the classical SPM reproduces the essential features of the quantum SPM. Note that  $M=33$  implies  $\lambda \approx a/4$ , which seems to be sufficient to yield good QCC. For the  $M$  system we also used  $M=33$ , however, since here  $2d/a=20$ , then  $\lambda$  is only slightly less than  $a$  ( $\lambda=0.6a$ ) and consequently the classical SPM showed important differences from the quantum one, ascribed to Heisenberg's uncertainty principle. It is important to remark that good QCC depends not on the type of dynamics (global or mixed chaos) but on the condition  $\lambda/a \ll 1$  or, equivalently,  $M \gg 2d/a$ . Thus, it is possible to have such a condition satisfied for channels that display mixed chaos, e.g.,  $\lambda/a \ll \frac{1}{4}$ .

### V. CONCLUDING REMARKS

We have studied quantum scattering properties of typical waveguides with mixed and global chaos by examining the quantum *scattering probability matrix* (SPM) and its classical counterpart. We emphasize that the definition of the classical SPM does not include any semiclassical aspects. We showed that the structure of the classical SPM allows us to predict the global structure of the quantum SPM. Since features of the classical SPM can be understood by the analysis of the trajectories, it was possible to understand the classical dynamical origin of important features of the quantum SPM. Consequently, the analysis of the classical SPM of a given electron waveguide system is useful for the understanding of its quantum transport properties, e.g., conductance. Plots of the classical SPM can be examined quickly to determine the influence of the cavity on the various modes. For a given energy, some modes may show ballistic behavior while others may display diffusive transmission, as observed recently in Ref. [25].

Our analysis of the quantum-classical correspondence of the SPM led us to discover the existence of “short-lived scars.” Specifically, we have seen that the wave function forms a ray pattern along the outgoing classical trajectory for modes corresponding to high-intensity elements of the clas-

sical SPM. They can be considered as short-lived scars because after a few bounces the ray pattern is destroyed by quantum interference.

Finally, we wish to mention that certain small but relatively high-intensity areas in the classical SPM led us to disclose the presence of extremely small Poincaré-Birkhoff structures of the otherwise globally chaotic billiard. Hence, the SPM gives complementary information to that obtained

solely by topological tools (e.g., Poincaré maps) since it is an intensity measure.

#### ACKNOWLEDGMENT

We wish to acknowledge financial support from CONACYT (Mexico) Grant No. 26163-E.

- 
- [1] J. R. Taylor, *Scattering Theory* (Wiley, New York, 1972); R. G. Newton, *Scattering of Waves and Particles*, 2nd ed. (Springer-Verlag, New York, 1982); H. Narnhofer and W. Thirring, *Phys. Rev. A* **23**, 1688 (1981).
- [2] W. H. Miller, *J. Chem. Phys.* **53**, 1949 (1970); **53**, 3578 (1970).
- [3] R. A. Marcus, *J. Chem. Phys.* **54**, 3965 (1971).
- [4] E. J. Heller, *J. Chem. Phys.* **65**, 4979 (1976).
- [5] P. Gaspard and S. Rice, *J. Chem. Phys.* **90**, 2225 (1989); C. Jung and S. Pott, *J. Phys. A* **23**, 3729 (1990); U. Smilanski, in *Chaos and Quantum Physics*, Proceedings of the Les Houches Summer School, Session LII, Course X, edited by M. J. Giamboni, A. Voros, and J. Zinn-Justin (Elsevier, New York, 1992); S. Kundoron, J. Delos, and B. Bloom, *J. Chem. Phys.* **83**, 5703 (1985); C. Jung and T. Tel, *J. Phys. A* **24**, 2793 (1991).
- [6] See, for example, *Mesoscopic Electron Transport*, Vol. 345 of *NATO Advanced Studies Institute, Series E: Applied Physics*, edited by L. L. Sohn, L. P. Kouwenhoven, and G. Schon (Kluwer Academic, Dordrecht, 1996); J. Imry, *Introduction to Mesoscopic Systems* (Oxford University Press, New York, 1997); S. Datta, *Electron Transport in Mesoscopic Systems* (Cambridge University Press, Cambridge, England, 1995).
- [7] R. Landauer, *IBM J. Res. Dev.* **1**, 223 (1957); **32**, 336 (1988); M. Buttiker, *ibid.* **32**, 317 (1988); *Phys. Rev. Lett.* **57**, 1761 (1986).
- [8] R. A. Jalabert, H. U. Baranger, and A. D. Stone, *Phys. Rev. Lett.* **65**, 2442 (1990); H. U. Baranger, R. A. Jalabert, and A. D. Stone, *Chaos* **3**, 665 (1993).
- [9] W. A. Lin, *Chaos, Solitons Fractals* **8**, 995 (1997).
- [10] See, e.g., C. M. Marcus, A. J. Rimberg, R. M. Westervelt, P. F. Hopkins, and A. C. Gossard, *Phys. Rev. Lett.* **69**, 506 (1992); C. M. Marcus *et al.*, *Surf. Sci.* **305**, 480 (1994); M. W. Keller *et al.*, *ibid.* **305**, 501 (1994); M. V. Berry *et al.*, *ibid.* **305**, 495 (1994); M. L. Roukes and O. L. Alerhand, *Phys. Rev. Lett.* **65**, 1651 (1990); C. W. J. Beenakker and H. van Houten, in *Solid State Physics*, edited by H. Ehrenreich and D. Turnbull (Academic, New York, 1991), Vol. 44, p. 1.
- [11] Gursoy B. Akguc and L. E. Reichl, *J. Stat. Phys.* **98**, 813 (2000).
- [12] R. Ketzmerick, *Phys. Rev. B* **54**, 10 841 (1996).
- [13] H. U. Baranger, D. P. DiVincenzo, R. A. Jalabert, and A. D. Stone, *Phys. Rev. B* **44**, 10 637 (1991); H. U. Baranger, R. A. Jalabert, and A. D. Stone, *Phys. Rev. Lett.* **70**, 3876 (1993); H. U. Baranger, *Physica D* **83**, 30 (1995).
- [14] E. Doron, U. Smilansky, and A. Frenkel, *Physica D* **50**, 367 (1991).
- [15] See, e.g., H-J. Stockmann, *Quantum Chaos: An Introduction* (Cambridge University Press Cambridge, UK, 1999), Sec. 2.2.
- [16] A. J. Lichtenberg and M. A. Leiberman, *Regular and Chaotic Dynamics*, 2nd ed. (Springer-Verlag, New York, 1992), Sec. (6.1b).
- [17] G. A. Luna-Acosta, A. A. Krokhin, M. A. Rodriguez, and P. H. Hernandez-Tejeda, *Phys. Rev. B* **54**, 11 410 (1996).
- [18] B. Huckestein, R. Ketzmerick, and C. H. Lewenkopf, *Phys. Rev. Lett.* **84**, 5504 (2000).
- [19] J. L. Tennyson, in *Nonlinear Dynamics and the Beam-Beam Interaction*, edited by M. Month and J. C. Herrera, AIP Conf. Proc. No. 57 (AIP, New York 1979), p. 158.
- [20] G. A. Luna-Acosta, K. Na, L. E. Reichl, and A. Krokhin, *Phys. Rev. E* **53**, 3271 (1996).
- [21] G. A. Luna-Acosta, J. A. Méndez-Bermúdez, and F. M. Izrailev, *Phys. Lett. A* **274**, 192 (2000).
- [22] G. A. Luna-Acosta, J. A. Méndez-Bermúdez, and F. M. Izrailev, *Phys. Rev. E* **64**, 036206 (2001).
- [23] B. Eckardt, *Physica D* **38**, 89 (1988); B. Eckardt and C. Jung, *J. Phys. A* **19**, L829 (1996); C. Jung, *ibid.* **23**, 1217 (1990).
- [24] H. U. Baranger, and P. A. Mello, *Phys. Rev. Lett.* **73**, 142 (1994).
- [25] J. A. Sánchez-Gil, V. Freilikher, I. Yurkevich, and A. A. Maradudin, *Phys. Rev. Lett.* **80**, 948 (1998).